

# Z-Contrast Imaging of Grain-Boundary Core Structures in Semiconductors

M.F. Chisholm and S.J. Pennycook

## Introduction

Interest in semiconductor grain boundaries relates to the development of polycrystalline materials for photovoltaics and integrated-circuit interconnects. Although these structures are responsible for deleterious electrical effects, there are few experimental techniques available to study them at the required atomic scale. Therefore models of the physical processes occurring at grain boundaries have necessarily taken a macroscopic approach. Fortunately recent developments have resulted in tools that provide unprecedented glimpses into these interfaces and that will allow us to address anew the connection between grain-boundary structure and properties.

## Z-Contrast Imaging

When exploring the unknown, we rely heavily on our eyes (incoherent imaging) to provide a direct image of a new object. In order to explore the unforeseen atomic configurations present at extended defects in materials, it again would be desirable if one could obtain a directly interpretable image of the unfamiliar structures present in the defect cores. Z-contrast electron microscopy provides such a view with both atomic resolution and compositional sensitivity.<sup>1</sup>

This high-resolution imaging technique differs from conventional high-resolution phase-contrast imaging. The phase-contrast technique produces a coherent image, an interference pattern formed by recombining the waves diffracted by the specimen. In the Z-contrast technique, the image is incoherent; it is essentially a map of the scattering power of the specimen. Additionally as was first

determined by Lord Rayleigh, the incoherent mode of image formation can double the resolving power of the coherent mode.<sup>2</sup>

Incoherent imaging with electrons is most easily implemented in a scanning transmission electron microscope. The Z-contrast image is obtained by scanning an electron probe of atomic dimensions across the specimen and collecting electrons scattered to high angles. The 100-kV and 300-kV microscopes used for the work described in this article are capable of producing electron probes of 0.22 nm and 0.13 nm, respectively. These probe diameters determine the resolution of the technique. The resulting map of the scattering power for the specimen is highly local, for it is mostly scattering produced close to the atomic nuclei that gets out to the high-angle annular detector.

The annular dark-field detector collects a substantial fraction of the scattered electrons and thus effectively averages over the phase relationships between diffracted beams leading to an image with incoherent characteristics. A direct correspondence exists between the object and its image, and there are no contrast reversals with sample thickness or objective lens defocus.<sup>3</sup> As long as the electron probe is smaller than the atomic column spacing and the inner detector angle is much larger than the beam convergence, the imaged atomic columns can be treated as independent scatterers. With this technique, unanticipated atomic arrangements present at defect cores will be directly revealed.

Additionally as the inner detector angle is increased beyond the minimum angle for transverse incoherence, the role

of thermal diffuse scattering in the imaging process increases, decreasing the coherence length along the atomic columns.<sup>4</sup> Thus the scattered intensity can approach the compositional sensitivity of the atomic-number-squared dependence of Rutherford scattering and allows detection of compositional inhomogeneities—for example, impurities segregated in the defect cores.

We have used this technique to explore the atomic arrangements present in silicon tilt grain boundaries. These examples illustrate the power of the technique to provide a unique and unambiguous image of defect cores, including several structures not previously anticipated.

## Models of Grain Boundaries

There are two general categories of grain-boundary models. The first was that of Quincke, who suggested the presence of an amorphous cement between grains.<sup>5</sup> The other view is that grain boundaries are best described as a crystalline zone between the lattices of two adjacent grains. Low-angle grain boundaries composed of an array of lattice dislocations became the defining structures of these models since the original suggestions by Taylor<sup>6</sup> and Burgers.<sup>7</sup> However at misorientations greater than about 15°, the separation of the required dislocations becomes so small that the description was thought to be unphysical.

Instead most high-angle grain-boundary models at present incorporate more complicated but still ordered transition zones to accommodate the misorientation. The most complete and accepted classification is the structural-unit model of Sutton and Vitek.<sup>8</sup> However as pointed out by Bishop and Chalmers in an earlier report about the model, the three descriptions of a grain boundary (an array of coincidence atoms, structural units, or dislocations) are in some sense equivalent.<sup>9</sup>

We will use the dislocation description, for as the following images demonstrate, the dislocation model remains a reasonable description of tilt grain boundaries in silicon, even at high tilt angles.

## [110] Tilt Boundaries

One of the most widespread applications of high-resolution phase-contrast electron microscopy has been the characterization of diamond-cubic semiconductors. Much of this attention has focused on the relatively open  $\langle 110 \rangle$  projection of this lattice and on its defects. In fact in the pioneering high-resolution-

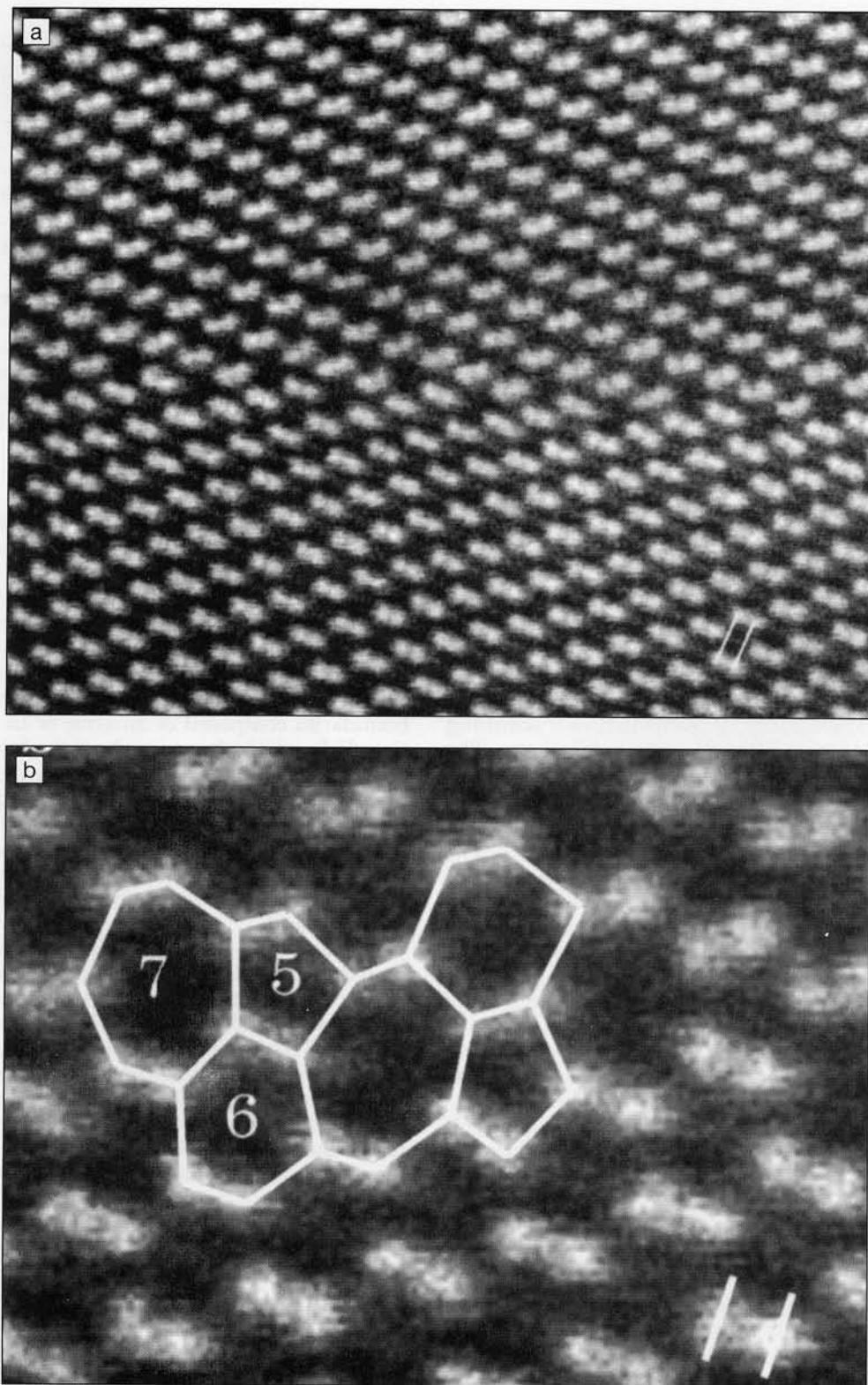


Figure 1. (a) Z-contrast image of a symmetric  $39^\circ \Sigma = 9 \{221\} \langle 110 \rangle$  silicon tilt grain boundary as viewed along the  $\langle 110 \rangle$  tilt axis. (b) A higher magnification view of the boundary showing the connected string of 5- and 7-membered ring structures present at its core. The separation between the parallel white lines in the images is 0.13 nm.

microscopy study of germanium published in 1977, Krivanek et al. correctly determined the atomic structure of a high-angle  $\langle 110 \rangle$  tilt boundary.<sup>10</sup>

Figure 1 is an image of the corresponding  $39^\circ \langle 110 \rangle$  symmetric tilt boundary in silicon as viewed 20 years later using the Z-contrast technique. The atomic-column positions are (always) the bright features in the Z-contrast image. In this  $\langle 110 \rangle$  projection, diamond-cubic crystals contain closely spaced pairs of atomic columns commonly referred to as "dumbbells." In silicon the projected separation of these two columns is 0.136 nm, and as seen in the image, they are resolved. The grain boundary, the region in which the misorientation of the two grains is accommodated, is extremely narrow. There are no dumbbells in intermediate positions.

The boundary contains a continuous string of 5- and 7-membered ring structures in place of the 6-membered rings of the perfect diamond-cubic lattice. This defect structure is identical to the core structure of a perfect edge dislocation with a  $\langle 110 \rangle$  line direction and an  $a/2\langle \bar{1}10 \rangle$  Burgers vector. The structure of this Lomer dislocation was first predicted by Hornstra in the 1950s.<sup>11</sup> There are no dangling bonds seen in this boundary. Bulklike tetrahedral bonding is maintained in the cores with relatively little distortion to the bond lengths or angles.

These dislocation cores can be packed one on top of the other and still remain distinct (see Figure 1). The edge dislocations have been found to be one of only two defects present in Si  $\langle 110 \rangle$  tilt boundaries. The other unit is the twin unit, a variation of the bulk 6-membered ring. If we can unravel the secrets of this dislocation, we will begin to unravel the secrets of boundaries with a  $\langle 110 \rangle$  tilt component as well. Along these lines, we have performed electronic-structure calculations on the  $a/2\langle 110 \rangle$  edge dislocation in silicon and have found the presence of states associated with the defects relatively deep in the gap ( $\sim 0.2$  eV) despite the absence of dangling bonds. The shifts in the electronic states are correlated with a concentration of strain in the cores.<sup>12</sup> The results of these calculations provide the first *ab initio* evidence that completely reconstructed dislocations can produce intrinsic gap states; dangling bonds and impurities are not required. The intrinsic band-tail states that have been measured would appear to be associated with the cores of "isolated" dislocations in grain boundaries (secondary dislocations and grain-boundary steps).<sup>13</sup>

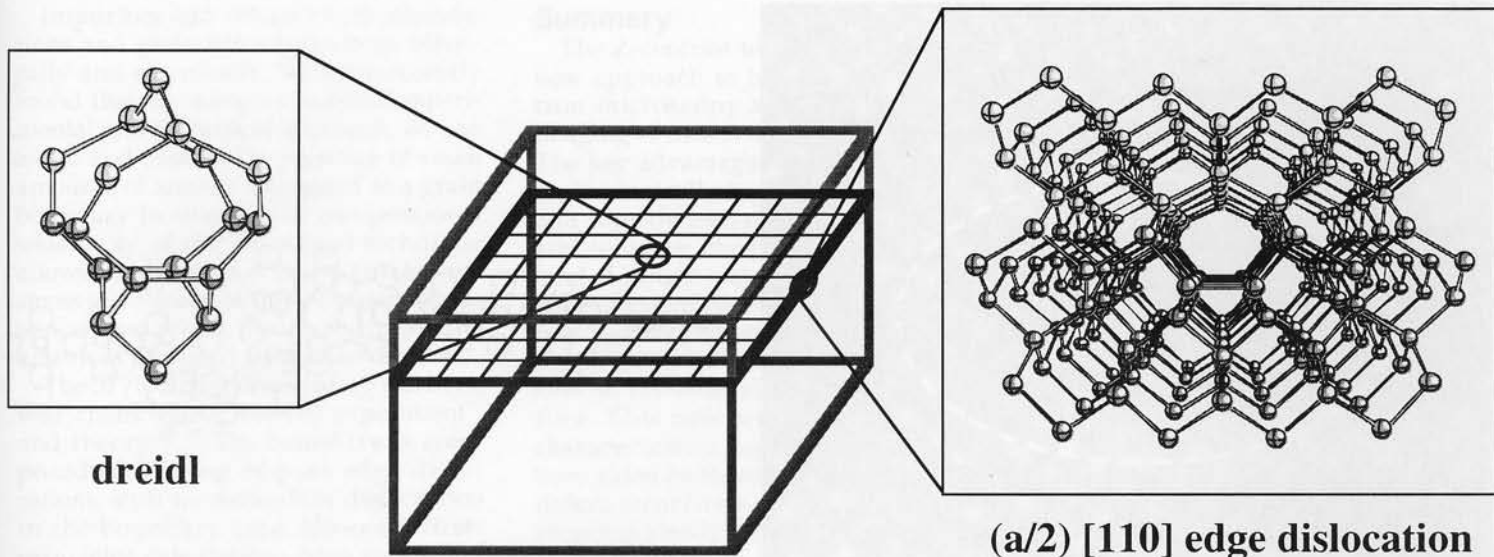


Figure 2. Schematic of an orthogonal array (center panel) of edge dislocations (right panel) and the resulting "dreidl,"—a low-energy, symmetric defect structure that forms at the dislocation intersections (left panel).

It is possible to construct a more random grain boundary by adding an orthogonal network of Lomer dislocations. As seen in Figure 2, these dislocations fit together, producing an intersection structure that resembles a dreidl and that again maintains tetrahedral bonding.<sup>14</sup> Similar "point defects" can be constructed for the intersections of other lattice dislocations as well. While this does not mean that all grain boundaries in diamond-cubic semiconductors are completely reconstructed to eliminate dangling bonds, it does indicate that grain boundaries of a more "random" kind can be assembled from the same defect structures seen in simple tilt grain boundaries.

### [001] Tilt Boundaries

There have been far fewer high-resolution investigations of  $\langle 001 \rangle$  tilt grain boundaries in diamond-cubic semiconductors. The principle reason for this is that instruments with point-to-point resolution better than 0.15 nm are required to reveal the structural features in these boundaries. Hornstra again predicted the building blocks contained in these boundaries long before microscopy had the tools to actually see them.<sup>15</sup> He proposed that any  $\langle 001 \rangle$  tilt boundary in diamond-cubic materials would be composed of arrays of two lattice dislocations. To date, only these two structural units have been seen in the boundaries but rarely in his proposed combinations.

Figure 3 shows the boundary structure, formed at a relatively low tilt angle of  $16^\circ$ , consisting of isolated defect cores

separated by perfect crystal units. These defect cores are asymmetric combinations of four identical units. In this  $\langle 001 \rangle$  projection, the individual units appear as a pentagon with an attached triangle. The closure failure around the entire defect is  $a[100]$ . This is the net Burgers vector and defect spacing expected for a  $16^\circ$  tilt boundary. However the defect core appears to be more complex than is necessary. There are twice the number of dislocations needed for this tilt angle, and the defects are clustered rather than uniformly spaced.

The boundary actually contains two of these asymmetric defect cores. The second is related to the first by a mirror across the  $\{170\}$  boundary plane and a glide. These two asymmetric defect cores have created somewhat of a dilemma for the boundary. The resulting structure is a compromise between achieving uniform spacing of the defect cores and maintaining a planar boundary.

Because strong image features do not reverse contrast through use of the Z-contrast technique, bright features can be directly interpreted as positions of atomic columns. However because the image is a two-dimensional projection, there is no information on the relative vertical positions of atoms in different columns. Molecular-dynamics simulations using the two-dimensional coordinates extracted from the image were used to determine the three-dimensional atomic arrangement present in the boundary. All the features of the image were reproduced in the simulation. From this three-dimensional structure, we see

that the four units are of a single dislocation type—an edge dislocation with Burgers vector  $\mathbf{b} = a/2[110]$  in a  $[001]$  line direction. Again we find the  $\langle 001 \rangle$  boundary cores can be described as arrays of closely spaced dislocations. Interestingly only two of these dislocations are required to accommodate the misorientation of the two grains. The other two unexpected units are arranged as a connected dislocation dipole with equal but opposite Burgers vectors and therefore are geometrically unnecessary.

Increasing the tilt angle to  $23^\circ$  produces another unforeseen atomic arrangement in which the entire boundary is composed of defect units (Figure 4). If the bulk-silicon positions are stripped from the image, the grain-boundary core consisting of a continuous string of pentagonal and triangular features remains. This  $\langle 001 \rangle$  projection has been used to calculate the three-dimensional structure of the defect. From the calculated grain-boundary core, two distinct structural units can be identified. These two units have the same atomic configuration as two known diamond-cubic lattice dislocations. These dislocation cores remain distinct; they have the same atomic configuration as they would have if isolated in the bulk crystal. The boundary dislocations do not mix or collapse even when spaced every 0.23 nm along the boundary.

The line direction of both dislocations is parallel to the boundary tilt axis. The units marked 1 and 1' in the schematic (Figure 4b) are the edge dislocations seen in the  $16^\circ$  boundary. The units marked 2, 2', 3, and 3' are mixed dislocations with

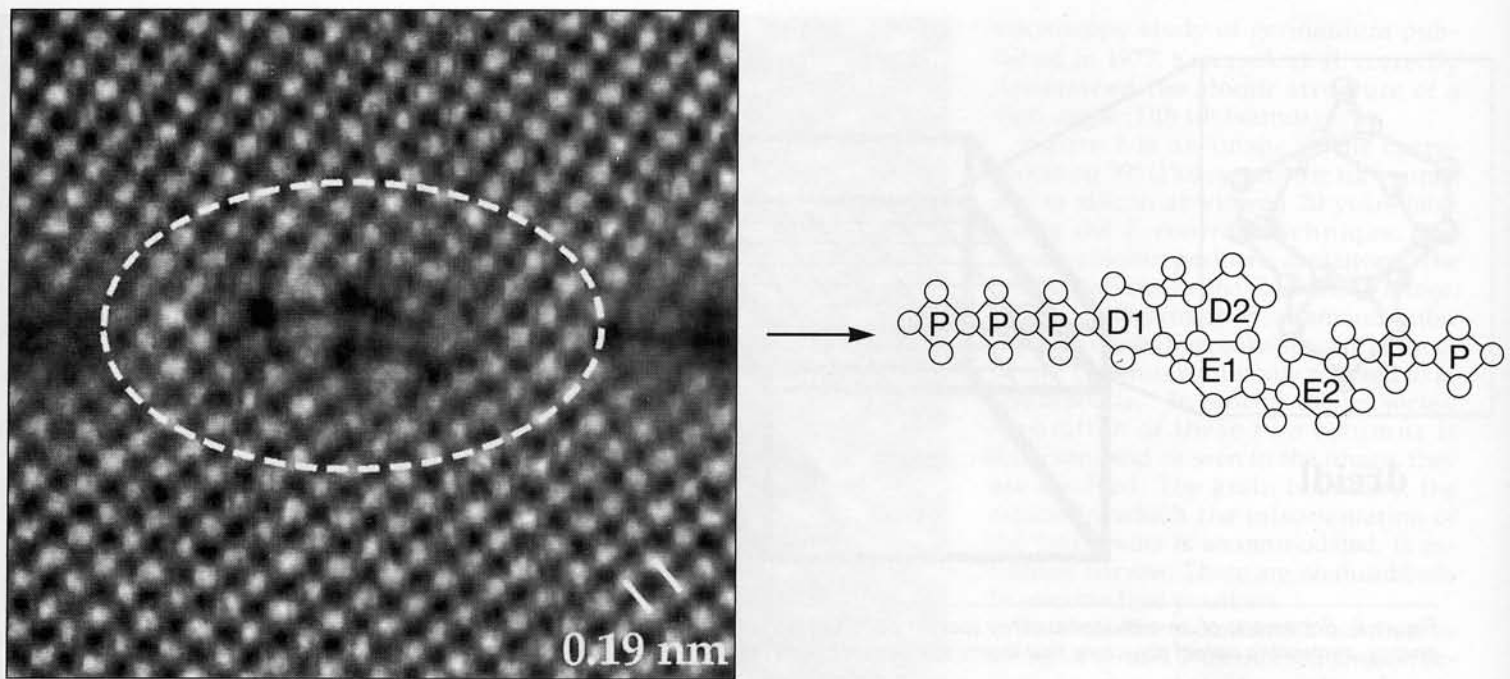


Figure 3. Z-contrast image of a symmetric  $16^\circ \Sigma = 25 \{170\} \langle 001 \rangle$  silicon tilt grain boundary as viewed along the bicrystal's common  $\langle 001 \rangle$  direction. The boundary consists of a periodic array of defect cores separated by relatively undisturbed crystal units. The closure failure around the defect core is  $a[100]$ . As seen in the schematic obtained directly from the image, the defect core consists of four identical units that in this projection appear as a connected pentagon-triangle pair. The units marked D1 and D2 are a connected dislocation dipole. The units marked E1 and E2 are the dislocations that accommodate the misorientation of the two grains.

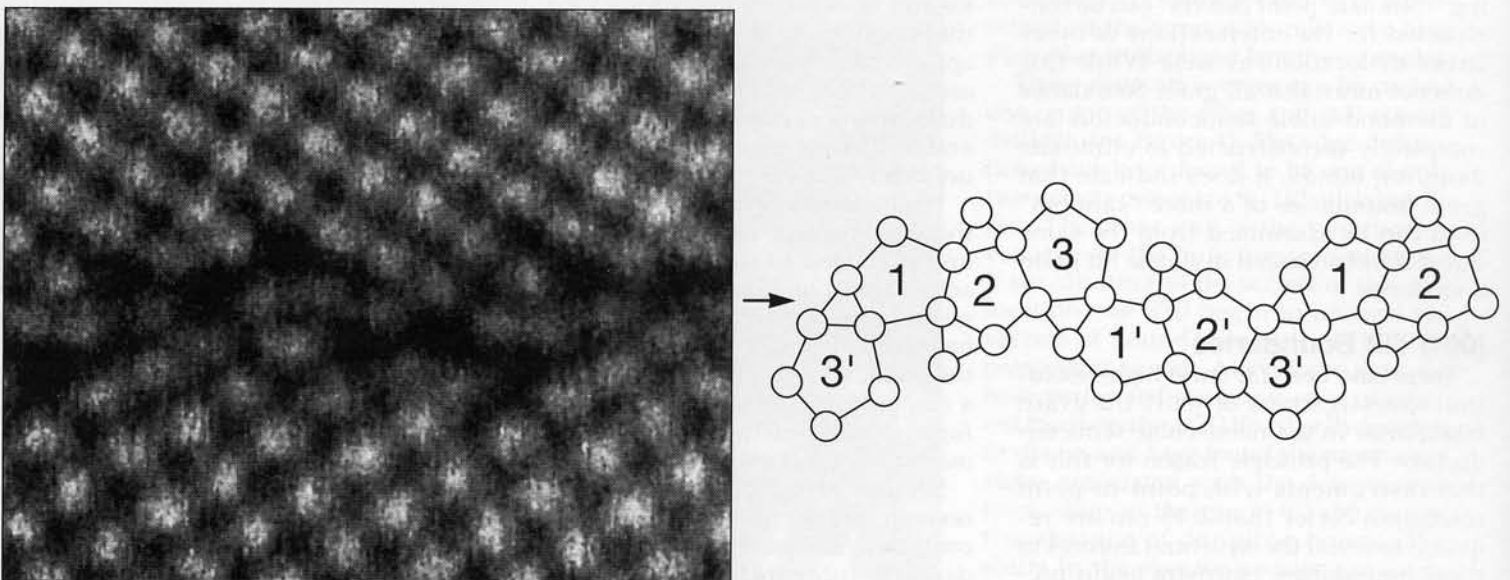


Figure 4. Z-contrast image of a symmetric  $23^\circ \Sigma = 13 \{150\} \langle 001 \rangle$  silicon tilt grain boundary and the projected atomic column positions obtained directly from the image. The boundary is seen to be periodic with a 1.38-nm repeat, containing two distinct units (edge dislocations, 1 and 1', and mixed dislocations, 2, 2', 3, and 3') arranged in a contiguous sequence of six dislocation cores. The bright features in the grains are separated by 0.19 nm.

equal edge and screw components. Their Burgers vector is inclined  $45^\circ$  to the  $\langle 001 \rangle$  plane. It is the presence of these mixed dislocations, arranged as dipoles, that is the unforeseen feature of this boundary.

As in the  $16^\circ$  boundary, the dipoles could be replaced by units of perfect crystal. The reason for these extra boundary dislocations is not obvious from classical potential calculations that indicate, while

the strain energy in the boundary is more uniform when the dipoles are present, there is little change to the total boundary energy. We await first-principles calculations to further explore this mystery.

Impurities can interact with dislocations and grain boundaries both elastically and electrically. We have recently found that, by using a combined experimental and theoretical approach, we can locate and explain the presence of small amounts of arsenic segregated to a grain boundary in silicon. The compositional sensitivity of the Z-contrast technique allows the detection of one or two arsenic atoms in a column of approximately 40 silicon atoms, while theory indicates the arsenic is arranged as isolated dimers.<sup>16</sup>

The 37° <001> Si tilt boundary has been well-characterized both by experiment<sup>17</sup> and theory.<sup>18-20</sup> The boundary is composed of a string of pure edge dislocations with no redundant dislocations in the boundary core. However first-principles calculations have raised the intriguing possibility that impurity segregation (specifically arsenic segregation) may drive a structural transformation of the boundary core.<sup>21</sup> This highlights the importance of being able to not only directly image the fine features of the defects but also to be able to detect the presence of impurities. Extended defects have a propensity to attract contaminants, and the impurities may be responsible for the observed atomic arrangement.

The investigation of <001> Si tilt boundaries using Z-contrast imaging has significantly reduced the perceived complexity of these defects. We have found no evidence of multiple grain-boundary structures coexisting in any of the boundaries we have examined. However the mystery of the redundant dislocations remains to be solved, for the goal is to predict the boundary structures without having to actually examine them.

## Summary

The Z-contrast technique represents a new approach to high-resolution electron microscopy allowing incoherent imaging of materials on the atomic scale. The key advantages of the technique—an intrinsically higher resolution limit and directly interpretable, compositionally sensitive imaging—provide a new level of insight into the atomic configurations of extended defects in silicon. Spectroscopic techniques can also be used to supplement the image, giving information on the local electronic band structure. This new level of experimental characterization has both stimulated and been aided by theoretical studies of these defect structures. This combined approach is ideally suited for investigations of defect states in semiconductors that control electronic properties, especially in identifying impurity segregation sites and their influence on the resultant atomic and electronic structure. Direct imaging of atomic arrangements combined with atomic-resolution chemical analysis has only begun to reveal and unravel the complexity of real materials at the atomic scale.

## Acknowledgments

We thank our theorist colleagues M. Mostoller, T. Kaplan, A. Maiti, and S.T. Pantelides for their important contributions to these investigations. This work was performed at Oak Ridge National Laboratory, which is managed by Lockheed Martin Energy Research Corporation under Department of Energy Contract No. DE-AC05-96OR22464.

## References

1. For example, see S. J. Pennycook, in *Handbook of Microscopy Methods II*, edited by S. Amelinckx, D. van Dyck, J. van Landuyt, and G. van Tendeloo (VCH, Weinheim, 1997) p. 595.
2. Lord Rayleigh, *Philos. Mag.* **42** (1896) p. 167.
3. S.J. Pennycook and D.E. Jesson, *Acta Metall. Mater.* **40** (1992) p. S149.
4. D.E. Jesson and S.J. Pennycook, *Proc. R. Soc. London, Ser. A* **449** (1995) p. 272.
5. G. Quincke, *ibid.* **76** (1905) p. 431.
6. G.I. Taylor, *ibid.* **145** (1934) p.388.
7. J.M. Burgers, *Proc. Kon. Ned. Akad. V. Wet. Amsterdam* **42** (1939) p. 293.
8. A.P. Sutton and V. Vitek, *Philos. Trans. R. Soc. London, Ser. A* **309** (1983) pp. 1, 37, 55.
9. G.H. Bishop and B. Chalmers, *Scripta Metall.* **2** (1968) p. 133.
10. O.L. Krivanek, S. Isoda, and K. Kobayashi, *Philos. Mag.* **36** (1977) p. 931.
11. J. Hornstra, *J. Phys. Chem. Solids* **5** (1958) p. 129.
12. F. Liu, M. Mostoller, V. Milman, M.F. Chisholm, and T. Kaplan, *Phys. Rev.* **51** (1995) p. 17192.
13. For example, see J. Werner, *Inst. Phys. Conf. Ser.* **104** (1989) p. 63.
14. M. Mostoller, M.F. Chisholm, and T. Kaplan, *Phys. Rev. Lett.* **72** (1994) p. 1494.
15. J. Hornstra, *Physica* **25** (1959) p. 409.
16. M.F. Chisholm, A. Maiti, S.J. Pennycook, and S.T. Pantelides, *Science* in press.
17. A. Bourret, J.L. Rouviere, and J.M. Penison, *Acta Crystallogr. Sec. A* **44** (1988) p. 838.
18. M. Kohyama, R. Yamamoto, Y. Ebata, and M. Kinoshita, *J. Phys. C* **21** (1988) p. 3205.
19. A.T. Paxton and A.P. Sutton, *ibid.* (1988) p. L481.
20. T.A. Arias and J.D. Joannopoulos, *Phys. Rev. B* **49** (1994) p. 4525.
21. A. Maiti, M.F. Chisholm, S.J. Pennycook, and S.T. Pantelides, *Phys. Rev. Lett.* **77** (1996) p. 1306. □